Earth Planet. Sci. Lett. 648 (2024) 119085

Contents lists available at ScienceDirect

Earth and Planetary Science Letters

journal homepage: www.elsevier.com/locate/epsl

The origin of tectonic mélanges from the Kodiak complex and Shimanto Belt and its implication for subduction interface processes

Kristijan Rajič [a,d,*], Hugues Raimbourg [a], Vincent Famin [b,c], Benjamin Moris-Muttoni [a]

[a] Institut des Sciences de la Terre d'Orléans, UMR 7327, Univ Orléans, CNRS, BRGM, OSUC, F-45071 Orléans, France
[b] Université de La Réunion, Laboratoire GéoSciences Réunion, F-97744 Saint-Denis, France
[c] Université Paris-Cité, Institut de physique du globe de Paris, CNRS, UMR 7154, F-75005 Paris, France
[d] Department of Earth Sciences, Durham University, Science Laboratories, South Road, Durham DH1 3LE, United Kingdom

ARTICLE INFO

Editor: Dr A Webb

Keywords:
Mélange
Subduction
Subduction interface
Contact metamorphism
Raman spectroscopy
IODP

ABSTRACT

Mélanges, intriguing rock units often found in accretionary complexes, consist of basalt lenses embedded in a highly sheared sedimentary matrix. The origin of mélanges remains a subject of vigorous debate, with consequences on our understanding of subduction processes. A first line of thought interprets mélanges as mixed lithologies intertwined by convergent tectonics. Supporters of this interpretation regard mélanges as fossilized witnesses of the lower- and upper-plate interface, with their rheological properties reflecting seismogenic subduction zones. However, a second line of thought is to consider that basalts and sediments were mixed prior to subduction by sedimentary and/or magmatic processes, this mix being only later incorporated into the accretionary wedge.

In this study, we present evidence supporting the pre-subduction mixing interpretation for mélanges from two paleo-accretionary complexes: the Kodiak complex in Alaska and the Shimanto Belt in Japan. In modern seafloor sediments in contact with basaltic submarine magmas, we show that the crystallinity of carbonaceous particles in sediments increases toward basalts, indicating a ~1 cm-thick aureole of contact metamorphism. Intriguingly, a comparable aureole of increased crystallinity is observed in four mélanges from the two paleo-accretionary complexes. Basalts were thus emplaced onto and into sediments by magmatism rather than by tectonics, challenging the notion of mélanges explored in this study as formed along the plate boundary interface. Moreover, the studied mélanges are made of mid-ocean ridge basalts, and deposition ages of mélange sediments coincide with proposed ridge subductions. This implies that the mid-ocean ridges at the trench were the source of the magmas that intruded into and extruded onto the clastic sediments and contributed to form the multilayered basalt-sediments architecture.

1. Introduction

Mélanges, characterized by their distinctive block-in-matrix structure with mafic blocks in a weaker sedimentary matrix, are a common feature of accretionary prisms (e.g., Festa et al., 2019). These intensely deformed rock units are often interpreted as exhumed subduction plate interfaces and are as such used to study many subduction-related processes including mechanical plate coupling, fluid-deformation interaction, and earthquake ruptures (Agard et al., 2018; Cloos and Shreve, 1988; Fagereng and Sibson, 2010; Kitamura et al., 2005; Moore and Byrne, 1987; Rowe et al., 2013). Nonetheless, other processes than tectonics may account for the mixing of lithologies. Pre-subduction, sedimentary mixing processes, where olistoliths originating from older accretionary prisms are redeposited in the trench, have been invoked in the Franciscan Belt in the USA (Wakabayashi, 2011) and the Nabae Belt in Japan (Osozawa et al., 2011). Alternately, the interlayering of mafic rocks and sediments might also reflect magmatic processes occurring on the seafloor prior to subduction (Kiminami et al., 1992; Kiminami and Miyashita, 1992).

In many instances, distinguishing these various processes is difficult because penetrative deformation erased the original organization of mafic and sedimentary lithologies. Nevertheless, the idea behind our study is that the second interpretation of magma emplacement into sediments should have left a thermal imprint, which is yet to be found.

* Corresponding author.
E-mail address: kristijan.rajic@durham.ac.uk (K. Rajič).

https://doi.org/10.1016/j.epsl.2024.119085
Received 27 February 2024; Received in revised form 12 September 2024; Accepted 15 October 2024
Available online 24 October 2024

Often, mélange-forming sediments are shales containing carbonaceous material (CM) whose crystallinity is dependent on peak metamorphic temperatures (Beyssac et al., 2002; Lahfid et al., 2010). As such, CM may serve as a potential record of contact metamorphism in sediments (e.g., Hilchie and Jamieson, 2014).

To assess the potential thermal influence of magmatism onto CM in sediments, we use a two-steps procedure. In the first validation step, we tested the possibility of identifying contact metamorphism from CM crystallinity in a simple case of undeformed seafloor sediments intruded by basaltic lavas/magmas. In a second step, we probed the existence of thermal anomalies at sediment-basalt contacts in five mélanges from the two paleo-accretionary complexes. Importantly, a tectonic origin of mixing has been invoked for the selected mélanges (Connolly, 1978; Ikesawa et al., 2005; Kimura et al., 2012; Kitamura et al., 2005; Moore and Byrne, 1987; Rowe et al., 2013; Yamaguchi et al., 2012). These mélanges experienced (sub)-greenschist facies metamorphism and were buried down to the seismogenic depths of subduction zones. Finally, we discuss the implications of our findings as for the formation of these low-temperature mélanges (i.e. <200–350 °C) and their significance in understanding subduction interface processes.

2. Geological settings and sampling strategy

2.1. Recent seafloor sediments intruded by basalts

Unconsolidated seafloor sediments in contact with basalts have been selected in three IODP/ODP drilling sites (Fig. A.1): (i) The Ninetyeast Ridge (ODP Leg 121, Hole 758A; Frey et al., 1991), (ii) The Shatsky Rise (IODP Leg 324, Site U1346; Sager et al., 2010), and (iii) The Hawai'i Emperor Volcanic Lineament (IODP Leg 197, Site 1204A; Tarduno et al., 2002). Basalt layers in these examples show size ranging from tens of centimeters up to few meters with an intrusive or extrusive origin (Text A.1). The distances of basalt layers near sediments at each site are indicated in Table A.1.

2.2. Mélange units from paleo-accretionary complexes

Five mélange units from the two paleo-accretionary complexes were selected (Table 1). The sediment-basalt contacts themselves present a variety of shapes, from serrated or folded surfaces to foliation-parallel planes or fault surfaces (Figs 1-2). As a precaution, we carefully selected sediment-basalt contacts in the less deformed parts of mélanges with no apparent fault or strain localization between the two lithologies (e.g., Figs 1-2), to avoid shear-induced heating as a cause of the thermal overprint of sediments (Kirilova et al., 2018; Moris-Muttoni et al., 2022). In parallel, reference samples of metasediments were collected as distant as possible from any basalts. The summary of each mélange is presented in Table 1, whereas the full list of samples is provided in Table A.2.

The Kodiak accretionary complex, Alaska, is a well-studied paleo-accretionary complex (Byrne, 1986; Fisher and Byrne, 1992) with NE-SW trending of units, parallel to the active Alaskan Trench (Plafker et al., 1994). The two mélanges of interest are the Uyak Complex (Connelly, 1978) and the Ghost Rocks mélange (Byrne, 1984, 1982). The locations of samples are provided in Figure A.3.

The Uyak Complex displays the block-in-matrix structure characterized by lenses of greywacke, chert and basalt within sheared argillitic layers (Fig. A.4; Connelly, 1978). Occasionally, the mélange displays a lack of deformation, with the preservation of pillow lavas (Fig. 1a-b). Stratigraphic ages from the Uyak Complex indicate a large time span of deposition from the Jurassic up to the Early Cretaceous (Clift et al., 2005; Connelly, 1978; Pavlis et al., 1988). Deformation and underthrusting is estimated to have occurred between the Valanginian and the Maastrichtian (Connelly, 1978). Fluid inclusion studies in Mode 1 veins indicate metamorphic temperatures of 270–290 °C and a pressure of 3.3 kbar (Vrolijk et al., 1988). In parallel, Raman Spectroscopy of carbonaceous material (RSCM) temperatures, measured at two localities of the Uyak Complex (Uyak Bay and Big Waterfall Bay, Fig. A.3), range between 240 and 260 °C in Uyak Bay (Raimbourg et al., 2021; Rajič et al., 2023a), and between 265 and 290 °C in Big Waterfall Bay (Rajič et al., 2023a). The analyzed pairs of samples come from Uyak Bay and Big Waterfall Bay (Fig. A.3).

The Ghost Rocks mélange is the southeastern part of the Ghost Rocks Formation otherwise made of coherent units and dated from the Paleocene (Byrne, 1982). The mélange consists of basalts and turbidites (Fig. 1c), which occasionally form a block-in-matrix structure (Fig. A.5). Pillow lavas shapes in basalts are sporadically preserved. Peak-metamorphic temperatures inferred from vitrinite reflectance, RSCM, and fluid inclusion studies correspond to 220–250 °C in Pasagshak and Sitkalidak areas (Moore et al., 1983; Rajič et al., 2023a; Vrolijk et al., 1988; locations in Fig. A.3) and 270–300 °C in Chiniak area (Rajič et al., 2023a). Based on fluid inclusion studies, pressure was estimated around ~3 kbar (Vrolijk et al., 1988). The selected samples of the Ghost Rocks mélange come from the Chiniak area (Fig. 1c-e), the Pasagshak area, and Sitkalidak Island (Fig. A.3).

The Shimanto Belt, Japan, represents a well-described paleo-accretionary complex (Taira et al., 1982, 1988) exposed on the islands of Honshu, Kyushu, and Shikoku in Japan (Fig. A.6a). It is composed of several parallel units with a general trend parallel to the active Nankai Trough (Fig. A.6a) and it contains several tectonic mélanges (e.g., Fig. A.6b). Three mélanges from the Shimanto Belt were selected for this study: The Foliated Morotsuka and the Hyuga Tectonic mélange were sampled at Kyushu Island, whereas the Mugi mélange is exposed on Shikoku Island (Fig. A.6).

The Foliated Morotsuka mélange consists of basaltic lenses embedded within a pelitic matrix (Fig. A7; Hara and Kimura, 2008; Ujiie et al., 2018). Biostratigraphic ages from the matrix range from the

Table 1
Summary of samples locations, deposition ages, and regional metamorphic temperatures of each studied mélange. RMT - regional metamorphic temperatures; RSCM – Raman Spectroscopy of carbonaceous material; VR - Vitrinite Reflectance; FI - Fluid inclusion studies; Mineral phase equilibria. References: 1 - Connelly (1978); 2 - Moore et al. (1983); 3 - Teraoka and Okumura (1992); 4 - Kiminami et al. (1992); 5 - Saito (2008); 6 - Rajič et al. (2023a); 7 - Vrolijk et al. (1988); 8 - Toriumi and Teruya (1988); 9 - Palazzin et al. (2016); 10 - Raimbourg et al. (2017); 11 - Rajič et al. (2023b); 12 - Ikesawa et al. (2005); 13 - Matsumura et al. (2003); 14 - Raimbourg et al. (2014).

Complex / *Unit*	Locality	Sample group	Longitude	Latitude	Deposition age	Ref.	RMT (°C)	Method	Ref.
Kodiak complex									
Uyak Complex	Uyak Bay	KO20	−154.00252	57.63912	Mid Permian-	1	240–260	RSCM	6
	Big Waterfall Bay	KO27	−152.53604	58.40956	Early Cretaceous		265–290	RSCM	6
Ghost Rocks mélange	Chiniak area	KO4	−152.20794	57.56351	Late Cretaceous-	2	280–300	RSCM	6
	Pasagshak area	KO13	−152.46035	57.42999	Early Palaeocene		220–250	RSCM; VR; FI	2, 6, 7
	Sitkalidak Island	KO47	−153.19103	57.20322			220–240	RSCM	6
Shimanto Belt									
Foliated Morotsuka	Kyushu	18NOB15–28	32.85311	131.97078	Cenomanian to Turonian	3	300–350	RSCM; MPE	8, 9, 10, 11
Mugi mélange	Shikoku	HN452–463	33.67068	134.44962	Early Palaeocene	4, 12	130–200	VR; FI	12, 13
Hyuga Tectonic mélange	Kyushu	18NOB07	32.52197	131.38422	Palaeocene-Middle Eocene	5	220–260	RSCM	9, 14

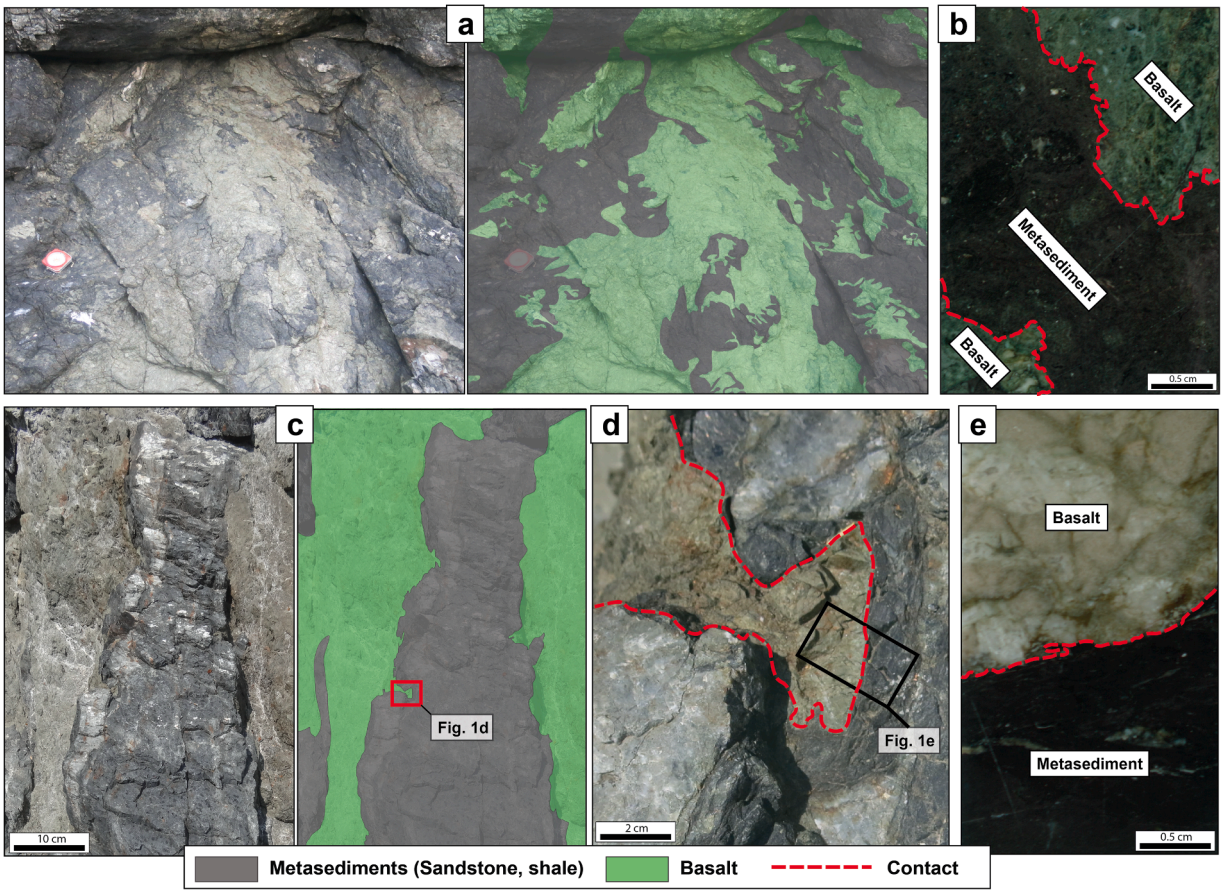

Fig. 1. Various contacts between metasediments and basalts in mélanges from the Kodiak accretionary complex, Alaska: (a) Irregular contact between massive sandstone and basalts without any obvious deformation structures, Uyak Complex. (b) A thick section showing sediment-basalt intercalation with irregular contacts (Sample KO20A). (c) Pillow lavas interlayered with sediment beds, Ghost Rocks mélange, with (d) small basalt injection within sediment bed characterized by a darker layer along the contact. (e) A thick section of the contact shown in (d).

Cenomanian to the Campanian/Maastrichtian (Teraoka and Okumura, 1992). The peak metamorphic conditions derived from mineral assemblages in metabasalts are 3–5 kbar and 300–350 °C (Toriumi and Teruya, 1988), while peak metamorphic temperatures inferred by RSCM in the pelitic matrix show the same temperature range (Palazzin et al., 2016; Raimbourg et al., 2017; Rajič et al., 2023b). Two types of basalt-shale contacts were sampled: (i) shale lenses surrounded by basalts (sample 18NOB28), and (ii) basaltic lenses in shale-dominant outcrops (18NOB15, 18NOB19, and 18NOB24). In both types, irregular and locally lobate contacts are observed, with a lack of tectonic contact between the two lithologies (Fig. 2a-b).

The Mugi mélange is of Late Cretaceous to Early Cenozoic age (Ikesawa et al., 2005; Kitamura et al., 2005; Shibata et al., 2008). The mélange consists of sandstone and basaltic lenses within a shale matrix (Kiminami et al., 1992; Kiminami and Miyashita, 1992; Yamaguchi et al., 2012). Peak metamorphic temperatures are in the range 130–200 °C, obtained by vitrinite reflectance and fluid inclusion studies (Ikesawa et al., 2005; Matsumura et al., 2003). The sampled contacts are lenses of sediments fully surrounded by basalts, often with preserved pillow lava shapes indicating limited strain (Fig. 2c).

The Hyuga Tectonic mélange is composed of blocks of sandstones and basalts scattered in a shaly matrix that shows a consistent foliation. Biostratigraphic ages in the Hyuga mélange range from the Late Eocene to the Early Oligocene (Sakai et al., 1984). The size of basaltic blocks ranges from mm- to m-scale (Raimbourg et al., 2019). Peak metamorphic temperatures range between 220 and 260 °C based on RSCM (Palazzin et al., 2016). Contacts between basalts and sediments are occasionally irregular (Fig. 2d). The studied samples (18NOB07C and 18NOB07D) are composed of basaltic fragments in a pelitic matrix, where the shale in contact with the basalt is darker than the shale away from the contact (Fig. 2d).

In those five mélange examples, the sediments, for all or a large proportion, are silico-clastic trench metasediments originating from the accretionary prism (Byrne, 1984; Connelly, 1978; Kiminami et al., 1992; Raimbourg et al., 2014; Shibata et al., 2008). In parallel, the basalts from the selected mélanges show a mid-ocean ridge (MOR) signature according to their chemical composition and textures (Byrne, 1984; Connelly, 1978; Kiminami et al., 1992; Kiminami and Miyashita, 1992; Kusky and Bradley, 1999; Mackenzie, 1989; Moore et al., 1983). These contrasted origins of sediments and basalts illustrate the conundrum of how mélanges are formed in convergent zones.

3. Methods

As there is no specific CM geothermometer designed for contact metamorphism, we employed RSCM methods calibrated for calculating regional metamorphic temperatures (Beyssac et al., 2002; Lahfid et al., 2010) to compare the Raman spectra of CM between contacting sediments and reference samples. RSCM were acquired using two instruments, a Raman Renishaw InVia Reflex micro-spectrometer at the ISTO-BRGM, Orléans, and a Renishaw InVia Qontor micro-spectrometer at CEMHTI CNRS, Orléans. The calibration was achieved using a silicon standard. The light source was a 514.5 nm Ar laser with an approximate power of 1 mV, and it was focused by a Leica DM2500 microscope at a magnification of 100x. Signal detection was carried out using a CCD NIR/UV detector.

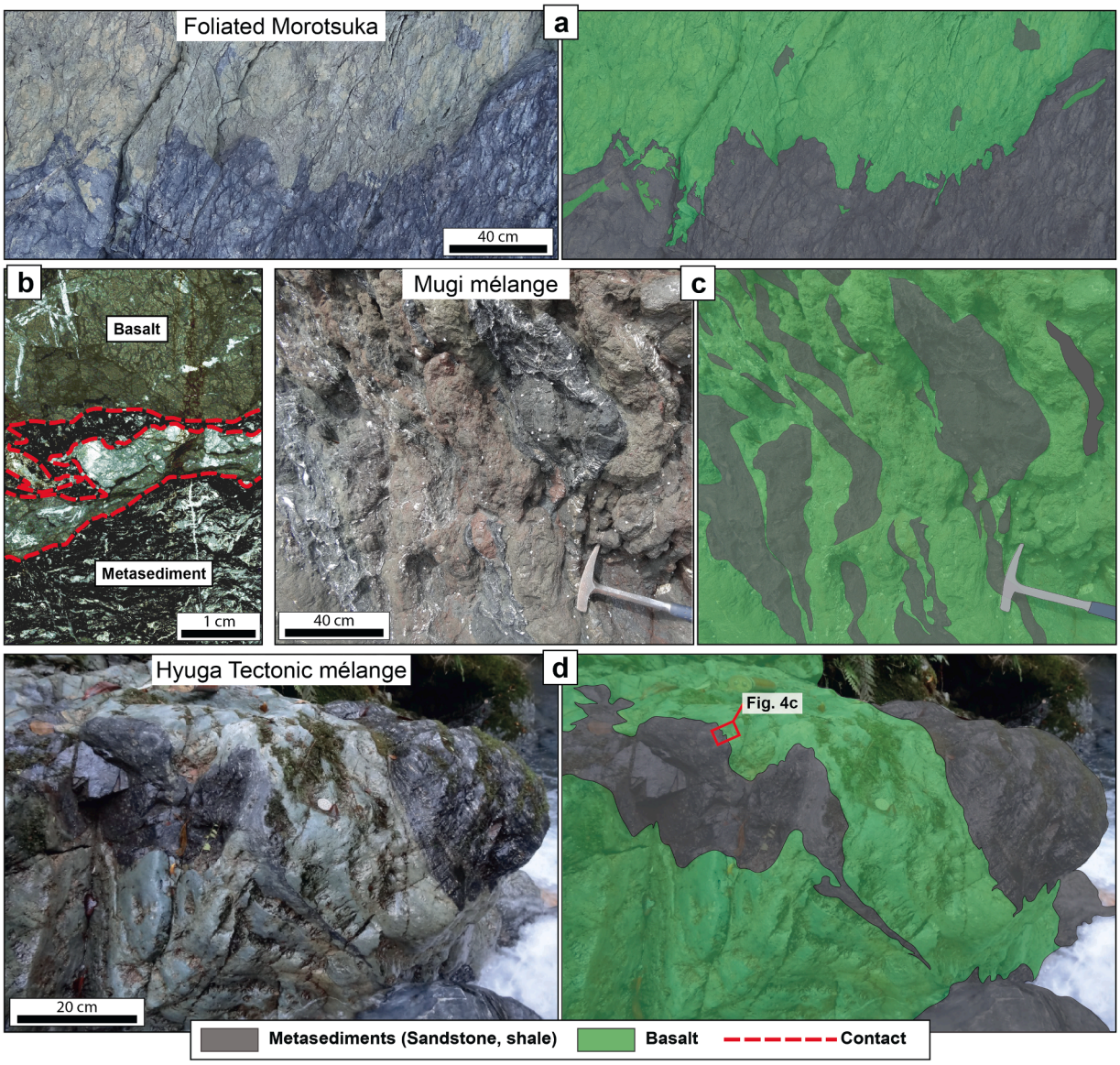

Fig. 2. Examples of irregular contacts observed in mélanges from the Shimanto Belt, Japan: (a) Irregular sediment-basalt contact in the Foliated Morotsuka. (b) A thick section showcasing sediment-basalt mixing in the Foliated Morotsuka (Sample 18NOB28B). (c) Lenses of sediments surrounded by pillow lavas, Mugi mélange. (d) Sediment-basalt mixed lithologies from the Hyuga Tectonic mélange.

Spot analyses of CM were performed on 200 μm-thick sections of the sampled sediment-basalt contacts. Points were spaced of 20 to 50 μm in the sediment matrix, and up to ~10 μm when approaching contact with the basalt. For reference sediment samples, CM was analyzed randomly throughout the thick sections, avoiding regions near shear bands to prevent any potential shear-induced effect on the CM (Kirilova et al., 2018; Moris-Muttoni et al., 2023).

Raman spectra were processed using the software PeakFit 4.12. Following the baseline subtraction and fitting of the resulting spectrum with five Lorenzian bands (D1 band at ~1350 cm^{-1}, G band at ~1580 cm^{-1}, D2 band at ~1620 cm-1, D3 band at ~1500 cm^{-1}, and D4 band at ~1200 cm^{-1}) or three Voigt functions (D1, D2, and G bands), depending on the Raman spectra shape and later processing. The choice of the method is extensively described in Rajič et al. (2023a). For points where five Lorenzian bands were applied, the RA1 ratio was derived following the equation: RA1 = (D1+D4) / (D1+D2+D3+D4+G), from which the peak metamorphic temperatures were calculated by RA1 = 0.0008 × T (°C) + 0.3758 (Lahfid et al., 2010). Samples from the Foliated Morotsuka experienced peak temperatures >300 °C and thus were treated following the method of Beyssac et al. (2002). The R2 ratio was calculated by the equation R2 = D1 / (D1 + D2 + G), later used to decipher peak temperatures T (°C) = 445 × R2 + 641. In selected samples from IODP/ODP expeditions, the Raman spectra were acquired without any additional deconvolution steps.

4. Results

In the three examples of undeformed pelagic sediments away from magmatic rocks, CM particles display Raman spectra characteristic of immature organic matter (Fig. 3). In sediments heated by a lava flow from the Hawai'i Emperor Volcanic Lineament, analyzed CM particles show a higher crystallinity within the 1-cm thick observed aureole than away from it, with complete graphitization (i.e., maximum crystallinity) in some particles (Fig. 3a). In sediments in contact with an intrusive basalt from the Ninetyeast Ridge, the analyzed CM particles show a higher crystallinity within the ~20-cm thick aureole of contact metamorphism than outside this aureole (Fig. 3b, Fig. A.2). In the Shatsky Rise, where the basalt layer is the thinnest amongst the three examples

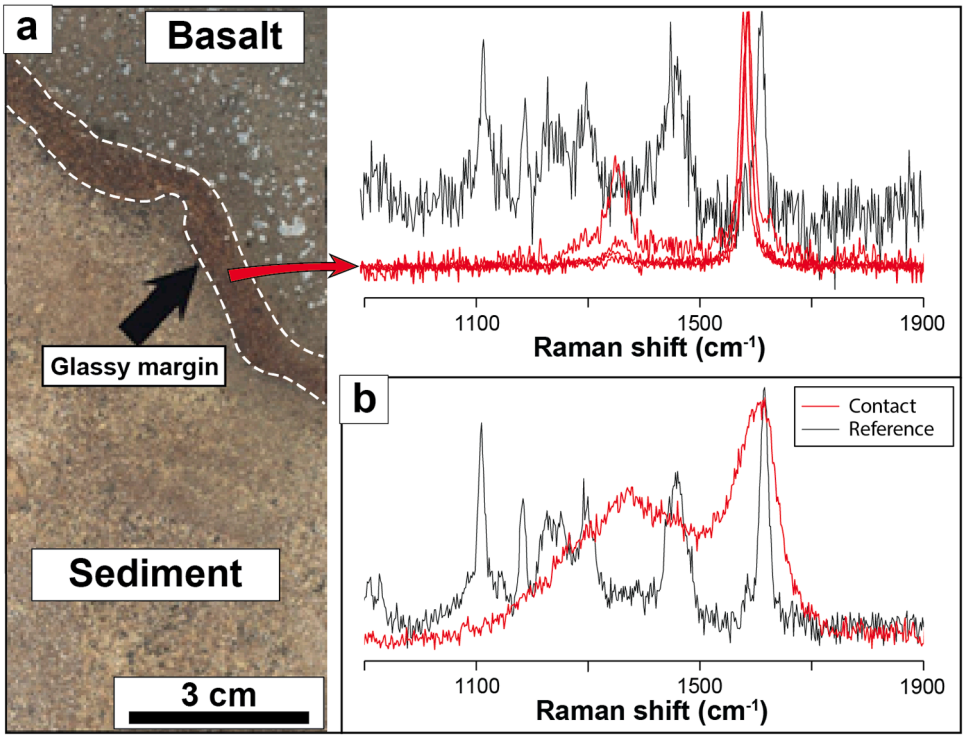

Fig. 3. (a) Example of sediment-basalt contact from Hawai'i Emperor Volcanic Lineament. The contact is a less than 1 cm-thick glassy margin, where Raman spectra of carbonaceous material (CM) suggest almost complete graphitization (red spectra), in contrast to highly disorganized CM in sediment further from the glassy margin (black spectra). (b) Examples of Raman Spectra of CM in sediments 20 cm away from the contact with basalt (black spectra) and within 1 cm from basalt (red spectra), Ninetyeast Ridge.

chosen, there is no visible effect of the basalt onto the CM in adjacent sediments (Fig. A.2).

Examples of Raman Spectra of CM in metasediments from paleo-accretionary complexes are illustrated in Fig. 4a. In four out of five mélanges, CM in metasediments in contact with basalts is characterized by notably higher RA1 values and inferred equivalent peak temperatures compared to reference samples away from basalts (Fig. 4b). The only difference between mélanges is the thickness of the contact rim.

In the Hyuga Tectonic mélange, RA1 values in both the reference and contact samples are relatively similar, except for CM located in close proximity to the basalt (up to 5 mm from the contact; Fig. 4c). RA1 values in the reference sample (18NOB7E) are of 0.56–0.60/0.56 (min-max/average). In the contact sample 18NOB07D (Fig. 4c), the CM within ~5 mm-thick contact with the basalt exhibits notably higher RA1 values compared to the metasediment further from the basalt, 0.59–0.66/0.60 compared to 0.56–0.60/0.58, respectively (Fig. 4b). In sample 18NOB7C, the ~5 mm-thick contact zone with basalt contain CM with RA1 values of 0.59–0.63/0.61, whereas in the section further away from the contact, RA1 values are of 0.56–0.60/0.58 (Fig. 4b).

In the Mugi mélange, metasedimentary lenses surrounded by pillow lavas (Fig. 2b) exhibit a wider thermal overprint (Fig. 4b). Four reference samples are characterized by the following RA1 min-max/average values: 0.46–0.55/0.50 in HN452; 0.46–0.60/0.54 in HN454; 0.48–0.59/0.53 in HN456; and 0.460.55/0.52 in HN457. Comparing RA1 results in reference samples from the Mugi mélange, it becomes evident that the thermal impact extends over tens of meters extensive basaltic occurrences (Fig. A.6d). In the metasedimentary lenses surrounded by pillow lavas (contact samples), average RA1 values are higher than in the reference samples (Fig. 4b): 0.550.68/0.59 in HN458; 0.52–0.70/0.59 in HN459; 0.54–0.67/0.60 in HN462; and 0.47–0.61/0.56 in HN463.

In the Ghost Rocks mélange, the thermal rim is restricted to at least 2 cm (on the thick section scale), observed in three groups of samples. In the Chiniak area, the reference sample (KO4C) has min-max/average RA1 values of 0.55–0.61/0.59, as opposed to RA1 values of 0.60–0.62/0.61 and 0.59–0.63/0.61 in contact samples (KO4B and KO4D, respectively). In the Pasagshak area, the reference sample (KO13C) displays min-max/average RA1 values of 0.53–0.58/0.55, whereas contact samples yield RA1 values of 0.56–0.64/0.59 and 0.56–0.68/0.58 (KO13A and KO13B, respectively). At Sitkalidak Island, the reference sample (KO47) has min-max/average RA1 values of 0.53–0.56/0.55, notably lower than the RA1 values of 0.56–0.61/0.60 and 0.57–0.63/0.60 found in contact samples (KO47C-1 and KO47–2, respectively).

In the Uyak Complex, RA1 values in the contact and referent samples remain similar, except for a few values in the immediate vicinity of basalts. Min-max/average RA1 values in the reference sample are of 0.54–0.58/0.56 (KO23), comparable to those of 0.57–0.59/0.58 in the contact sample (KO20A). The situation is similar in Big Waterfall Bay, with a reference sample (KO25F) at 0.58–0.60/0.59 min-max/average RA1 values. In the contact sample (KO25E), RA1 values are 0.58–0.60/0.59 away from the contact, whereas in the ~5 mm-thick contact with basalt, RA1 values are of 0.59–0.67/0.62 (Fig. 4d).

In the Foliated Morotsuka, regional metamorphic temperatures are higher than in other mélanges (>300 °C), and thus R2 ratio from Beyssac et al. (2002) was calculated. Here, no differences have been observed between contact and reference samples, except for a few points with R2 ratio being below 0.50 (Fig. A.8).

5. Discussion

5.1. Origin of sediment-basalt mixing

Several processes have been proposed for the formation of mélanges worldwide (e.g., Festa et al., 2019): (i) along the plate boundary interface or during basal underplating, involving tectonic mixing and deformation (Agard et al., 2018; Cloos and Shreve, 1988; Fagereng and Sibson, 2010; Kitamura et al., 2005; Moore and Byrne, 1987; Rowe et al.,

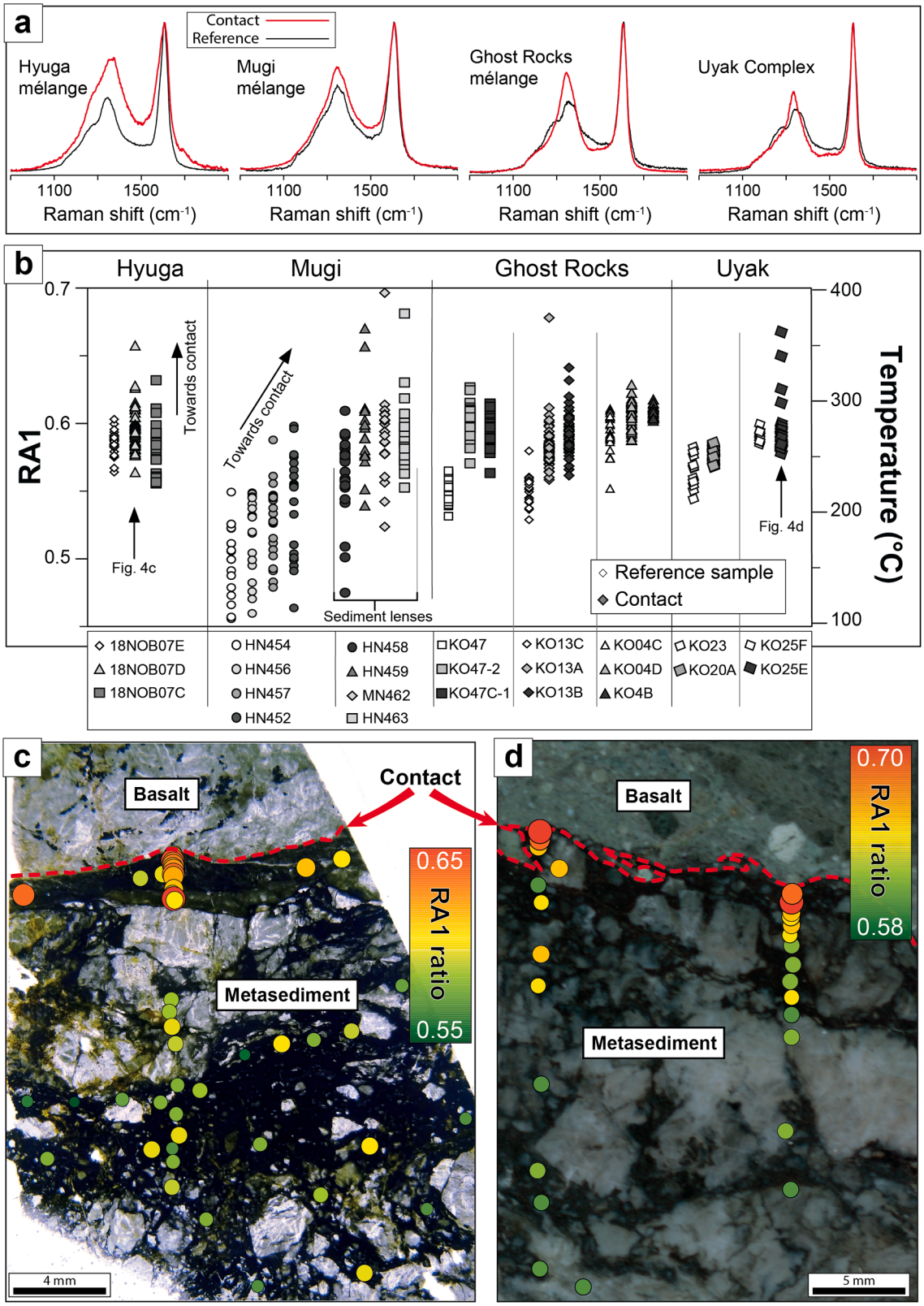

Fig. 4. (a) Examples of Raman spectra of CM from mélanges in Japan (Hyuga and Mugi mélanges) and in Alaska (Ghost Rocks mélange and Uyak Complex). Black and red spectra are representative of CM from metasediments away from basalts and in contact with basalts, respectively. (b) The compilation of RA1 ratios of analyzed CM and calculated "apparent" temperatures for each mélange. White symbols represent results from reference samples, whereas adjacent gray symbols represent samples of sediment in contact with basalt. (c-d) A closer look into RA1 ratios in samples from (c) the Hyuga mélange (18NOB07D) and (d) Uyak Complex (KO25E), showing systematically higher values close to the contact compared to a few mm away from the basalt.

2013); (ii) pre-subduction sedimentary mixing processes with localized syn-subduction deformation (Wakabayashi, 2011; Osozawa et al., 2011); (iii) the interlayering of mafic rocks and sediments by magmatic processes on the seafloor prior to subduction with localized syn-subduction deformation (Kiminami et al., 1992; Kiminami and Miyashita, 1992). For the studied mélanges, it is widely accepted that they formed along the plate boundary interface and/or during underplating, as evidenced by the presence of highly deformed sections characterized by noncoaxial deformation with a top-to-the-trench sense of shear (e.g., Connolly, 1978; Ikesawa et al., 2005; Kimura et al., 2012; Kitamura et al., 2005; Moore and Byrne, 1987; Rowe et al., 2013; Yamaguchi et al., 2012). However, some sections of the mélanges exhibit minimal deformation with an absence of fault contact between the sediments and basalts (Fig. 1-2). This raises a main question: how can these mélanges contain both block-in-matrix structure and coherent portions with mildly deformed sediments and basalts?

The findings of this study reveal that CM in pelagic sediments captures the thermal effects resulting from interactions with magmas, up to extreme cases where CM has undergone nearly complete graphitization (Fig. 3a). Two of the three studied seafloor examples (Hawai'i and the Ninetyeast Ridge) of pelagic sediment-magma interaction record evidence of contact metamorphism, both in mid-ocean ridge and hotspot contexts, and both in intrusive and extrusive cases of magma emplacement (Text A.1). In the third case study, the Shatsky rise, no evidence of increased CM crystallinity was found in the sediments adjacent to basalts. This implies that, even though mixing occurred on the seafloor, the imprint of contact metamorphism is not systematically recorded in the surrounding sediments.

Remarkably, a thermal overprint is also preserved in our selected mélange samples from paleo-accretionary complexes, despite undergoing low-grade metamorphism. In four out of five mélanges from this study, the RA1 ratio is higher in CM in metasediments in contact with basalts than in reference samples (Fig. 4b). The scale of the contact aureole recorded by the CM ranges from a few millimeters in the Hyuga mélange and the Uyak Complex, to a few centimeters in the Ghost Rocks mélange, and up to several meters in the Mugi mélange. Our careful selection of sediment-basalt contacts, based on the absence of strain localization (Figs 1-2), eliminates the eventuality that the crystalline structure of the CM has been affected by shear-induced heating along fault zones (Kirilova et al., 2018; Moris-Muttoni et al., 2022, 2023; Rowe et al., 2005).

Consequently, the RSCM anomalies found in mélange sediments adjacent to mafic bodies is best explained by the emplacement of hot basaltic magmas into or onto the trench sediments (Fig. 5a). This scenario implies that the intermingling of basalts and sediments occurred because of magmatic processes during sedimentation in the trench rather than due to tectonic or sedimentary processes (Kimura et al., 2012; Kitamura et al., 2005; Osozawa et al., 2011; Tulley et al., 2020). The original contacts inherited from the magmatic emplacement may be then erased during subduction burial of these units. During subduction or underplating, these mixed lithologies undergo varying degrees of deformation (Fig. 5a) influenced by factors such as the sediment-to-basalt ratio (Fagereng and Sibson, 2010), and likely their proximity to the plate boundary interface where strain is most intense. Thus, pre-subduction mixing together with syn-subduction deformation provide the most plausible explanation for the presence of both heavily

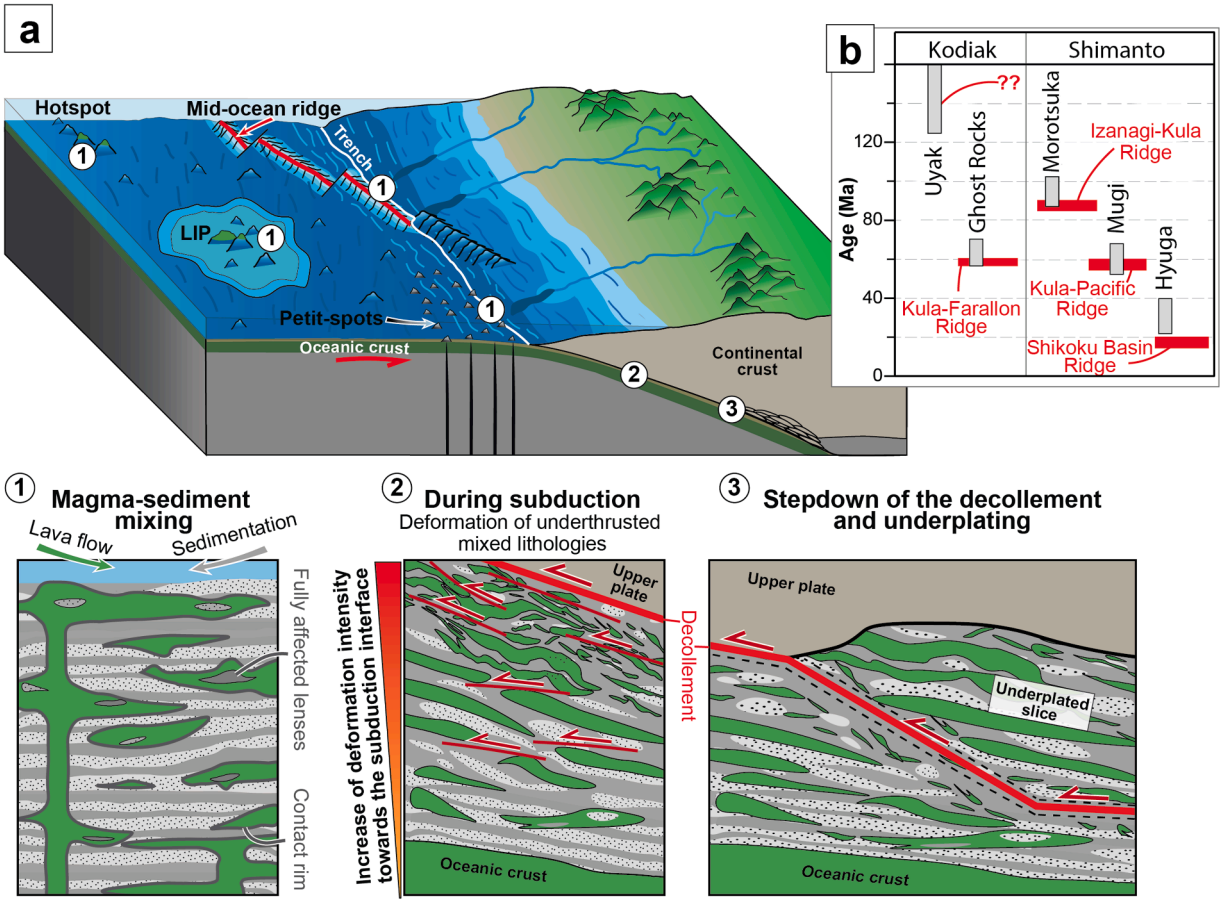

Fig. 5. (a) Model of mélange evolution from deep seafloor down to the base of the accretionary prism. (1) Basalt-sediment mixing on the ocean floor occurs in a variety of contexts: hotspots, large igneous provinces (LIP), petit-spots, and mid-ocean ridges. (2) Underthrusted sequence experienced varying degrees of deformation intensity depending on its proximity to the subduction interface. (3) Stepdown of the decollement and underplating of mélange slices. (b) Deposition ages of each mélange from the Kodiak complex and the Shimanto Belt (gray boxes), with previously proposed ridge subduction events in both complexes (red boxes).

deformed segments and comparatively undeformed sections within mélanges found in exhumed complexes.

The main limitation of the method is that the thermal influence of basalts on sediments is likely to be overprinted by subsequent regional metamorphism. Given the irreversible nature of CM transformation (Beyssac et al., 2002), the imprint of contact metamorphism on CM persists as long as regional metamorphism does not overprint the record of the early contact metamorphism event. All examples where a RSCM anomaly was observed were buried down to conditions of regional metamorphic temperatures lower than 300 °C (Fig. 4). This may explain the lack of preserved contact metamorphism in the Foliated Morotsuka. In this mélange, the peak metamorphic temperatures range between 300 and 350 °C (Raimbourg et al., 2017; Rajič et al., 2023b; Toriumi and Teruya, 1988), higher than in the other studied mélanges. Indeed, the CM structure within the contact rim documents temperatures that align with regional metamorphism reaching up to 350 °C (with only a few points corresponding to temperatures of up to 400 °C; Fig. 4b). Thus, sufficiently high regional metamorphic temperatures may erase the thermal anomalies of pre-subduction contact metamorphism.

5.2. The possible sources of basalts

The critical question that arises from our RSCM results is to explain how basalts may be emplaced in trench sediments prior to subduction. Various sources of magmatic rocks, including hotspots or large igneous provinces, produce large quantities of lavas which can mix with nearby sediments (Ernst, 2014; Jellinek and Manga, 2004; Fig. 5a). In the selected mélanges, however, RSCM results show that the basalts have been emplaced within the trench sediments, which limits the possible magmatic sources. Among such magmatic sources are petit-spots caused by the lithospheric flexure at the nearby trench (Hirano, 2011). In the Japan subduction zone for example, petit-spot volcanoes are reported in the very vicinity to the trench (Hirano, 2011; Hirano et al., 2019), which makes them plausible sources for the emplacement of lavas within trench sediments. Moreover, in sediments near the Japan Trench, the disturbance of sediment layers by petit-spot magmas is reported, with a thermal aureole in sediments in contact with magmas (Akizawa et al., 2022). Petit-spots are discovered to occur in other subduction zones as well, such as in Chile or Java (Hirano and Machida, 2022), meaning that they are likely a general feature of subduction zones. Petit-spot lavas have been identified as well in the exhumed complex of Central Chile (Munoz-Montecinos et al., 2024), indicating the mixing of petit-spot lavas and sediments in deep trench environments. However, petit-spot lavas are characterized by a distinct chemical composition that differs from MOR basalts (Hirano, 2011; Munoz-Montecinos et al., 2024). Therefore, additional geochemical analyses of mafic rocks in exhumed mélanges are necessary to fully assess their significance.

The last important source of basaltic lavas are mid-ocean ridges. As mentioned earlier, basalts from the selected mélanges are all interpreted as MOR lavas (Byrne, 1984; Connelly, 1978a; Kiminami et al., 1992; Kiminami and Miyashita, 1992; Kusky and Bradley, 1999; Mackenzie, 1989; Moore et al., 1983). Moreover, in the Uyak Complex and its prolongation to the northeast in mainland Alaska (the McHugh Complex, Kusky and Bradley, 1999; Plafker et al., 1994), highly deformed basaltic lenses are characterized as well by a MOR chemical composition and geochemically indistinguishable from massive and pillow basalts in the same complex (Connelly, 1978; Kusky and Bradley, 1999), suggesting that highly deformed lenses have likely the same origin as undeformed pillow basalts from the same unit.

The preservation of MOR basalts thermally affecting trench sediments suggests that the studied mélanges represent a record of an active mid-ocean ridge in proximity of the trench where the sedimentation occurred. The proximity of mid-ocean ridge to the deposition site is particularly adapted to explain the very large lateral extent of some mélanges, such as in Alaska, running as a trench-parallel continuous formation over >500 km from the Uyak Complex to the McHugh Complex (Kusky and Bradley, 1999; Plafker et al., 1994). This observation would be otherwise very difficult to explain by another source of magmatism.

Indeed, several events of ridge subduction or trench-ridge interaction have been proposed in the studied complexes (Fig. 5b). In the Shimanto Belt, these events include (1) the Kula-Izanagi ridge subduction at 90–85 Ma (Aoki et al., 2012; Saito et al., 2014), (2) the Izanagi-Pacific ridge subduction at 60–55 Ma (Müller et al., 2008; van de Lagemaat and van Hinsbergen, 2023), and (3) the Shikoku Basin ridge-trench interaction at 20–15 Ma (Ali and Moss, 1999; van de Lagemaat and van Hinsbergen, 2023). The first two events correspond to the deposition age of the Foliated Morotsuka (Maruyama and Send, 1986; Teraoka and Okumura, 1992) and the Mugi mélange (Kimura et al., 2012), respectively. As regards the third, most recent one, the ridge subduction postdates the deposition ages of the sediments that constitute the Hyuga mélange (Nishi, 1988; Sakai et al., 1984), so the question of the origin of the basalts the mélange remains open. In the Kodiak complex, the Kula-Farallon ridge subduction was proposed at 60–58 Ma (Farris and Paterson, 2009), contemporaneous to the deposition of the Ghost Rocks mélange (Moore et al., 1983). Therefore, mid-ocean ridge subduction events temporally coincide with the timing of trench sediment deposition in three of the five mélanges examined in this study, indicating that the basaltic source was indeed proximal to the deposition site.

5.3. Implications for subduction processes

Within accretionary prisms, the typical sequence of lithologies from a basaltic sole to pelagic cherts and clays topped by trench siliciclastics upwards, define the oceanic plate stratigraphy (OPS) interpreted as the upper level of the lower plate undergoing subduction (Taira et al., 1988; Wakabayashi, 2017). OPSs are further characterized by younging biostratigraphic ages towards the top of the sedimentary pile. The discovery of repeated OPSs, in the Franciscan Complex (Meneghini and Moore, 2007), US California, and the Shimanto Belt (Taira et al., 1988), has led to the concept of tectonic underplating at the bottom of accretionary wedges. This concept involves down-stepping of the decollement fault (i.e. the interface between the lower- and upper plates, see Fig. 5a) into the top of the basaltic crust (e.g., Angiboust et al., 2021; Menant et al., 2020). The step-down, or downward migration of the decollement, scraps off slivers of the down-going plate and add them to the upper plate, leading to an imbricated structure of sediment-basalt slivers.

Some authors have generalized this concept and proposed to explain mélanges by tectonic underplating (Kimura et al., 2012; Kimura and Mukai, 1991; Saito, 2008; Sample and Fisher, 1986), even when the full sedimentary sequence is not present (such as all examples, but for the Uyak Complex treated here, as pelagic cherts are absent or very rare) and when the relationship between the mafic and sedimentary layers or slivers is obscured by strain. One argument against this model in mélanges from the Shimanto Belt is the kinematics of the deformation within the mélange, dominated by extension and not by shortening (Raimbourg et al., 2019). Furthermore, in the same belt, radiometric dating showed that several mélange-bounding faults were active long after underplating, and hence could not be interpreted as down-steps of the decollement (Fisher et al., 2019). The thermal record of trench sediments interlayered with basalts in the examples studied here point to an alternative pre-subduction model of formation, where the basalt-sediment lithological alternations are inherited from magmatic-sedimentary processes at the trench, with syn-subduction deformation locally affecting the architecture of such mixed lithologies.

6. Conclusion

In this study, Raman Spectroscopy of carbonaceous material was employed to detect a potential record of contact metamorphism in sediment-basalt mixed lithologies. In two recent examples of magmas

emplaced in pelagic sediments, the thermal impact from basalt caused the crystallinity of carbonaceous material to increase almost to full graphitization, demonstrating the ability of RSCM to detect short-lived contact metamorphism even in seafloor, porous sediments.

Such record is also preserved in four mélanges from two paleo-accretionary complexes in Alaska and Japan, suggesting that the basalts were emplaced within trench sediments prior to subduction. Given the MOR signature of the basalt, our preferred scenario is that the selected mélanges represent remnants of active mid-ocean ridges that disappeared into subduction. As a result, the studied mélanges retrieved from the two accretionary prisms cannot be considered as a direct image of the tectonic processes that happen along the subduction plate interface, in particular its seismogenic portion. For example, tectonic mélanges such as Mugi in Japan and Ghost Rocks in Alaska do not simply reflect the structure and thickness of the plate subduction interface, as proposed by Rowe et al. (2013), but a complex combination of pre-subduction geometry and tectonic processes during burial and exhumation. Our study suggests a simpler picture, where the variable proportion of basalts may be inherited from the original magmatic context on the seafloor.

CRediT authorship contribution statement

Kristijan Rajič: Writing – original draft, Software, Methodology, Investigation, Formal analysis, Data curation. **Hugues Raimbourg:** Writing – review & editing, Supervision, Resources, Project administration, Methodology, Funding acquisition, Data curation, Conceptualization. **Vincent Famin:** Writing – original draft, Project administration, Investigation, Funding acquisition, Data curation. **Benjamin Moris-Muttoni:** Writing – review & editing, Software, Methodology, Investigation, Formal analysis, Data curation, Conceptualization.

Declaration of competing interest

The authors declare that they have no known competing financial interests or personal relationships that could have appeared to influence the work reported in this paper.

Acknowledgments

We thank Old Harbor Native Corporation for the support during the field survey in Old Harbor area, D. Fisher and K. Morell for their help during fieldwork, S. Janiec for the preparation of thin sections, and A. Canizarés for analytical support with Raman Spectroscopy. Two anonymous reviewers are thanked for thoughtful comments and suggestions that improved the manuscript, as well as A. Webb for editorial handling. This study was funded by LabEx VOLTAIRE (ANR-10-LABX-100–01) and EquipEx PLANEX (ANR-11-EQPX-0036) projects.

Supplementary materials

Supplementary material associated with this article can be found, in the online version, at doi:10.1016/j.epsl.2024.119085.

Data availability

The Appendices can be accessed on Zenodo repository (10.5281/zenodo.11474344).

References

Agard, P., Plunder, A., Angiboust, S., Bonnet, G., Ruh, J., 2018. The subduction plate interface: rock record and mechanical coupling (from long to short timescales). Lithos. 320–321, 537–566. https://doi.org/10.1016/j.lithos.2018.09.029.

Akizawa, N., Hirano, N., Matsuzaki, K.M., Machida, S., Tamura, C., Kaneko, J., Iwano, H., Danhara, T., Hirata, T., 2022. A direct evidence for disturbance of whole sediment layer in the subducting Pacific plate by petit-spot magma–water/sediment interaction. Marine Geology 444, 106712. https://doi.org/10.1016/j.margeo.2021.106712.

Ali, J., Moss, S., 1999. Miocene intra-arc bending at an arc–arc collision zone, central. Japan: Comment. Island Arc 8, 114–123. https://doi.org/10.1046/j.1440-1738.1999.00218.x.

Angiboust, S., Menant, A., Gerya, T., Oncken, O., 2021. The rise and demise of deep accretionary wedges: A long-term field and numerical modeling perspective. Geosphere. https://doi.org/10.1130/GES02392.1.

Aoki, K., Isozaki, Y., Yamamoto, S., Maki, K., Yokoyama, T., Hirata, T., 2012. Tectonic erosion in a Pacific-type orogen: Detrital zircon response to Cretaceous tectonics in Japan. Geology. 40, 1087–1090. https://doi.org/10.1130/G33414.1.

Beyssac, O., Goffé, B., Chopin, C., Rouzaud, J.N., 2002. Raman spectra of carbonaceous material in metasediments: a new geothermometer: RAMAN SPECTROSCOPY OF CARBONACEOUS MATERIAL. J. Metamorph. Geol. 20, 859–871. https://doi.org/10.1046/j.1525-1314.2002.00408.x.

Byrne, T., 1986. Eocene underplating along the Kodiak Shelf, Alaska: Implications and regional correlations. Tectonics. 5, 403–421. https://doi.org/10.1029/TC005i003p00403.

Byrne, T., 1984. Early Deformation in Melange Terranes of the Ghost Rocks Formation. Geological Society of America Special Papers. Geological Society of America, Kodiak Islands, Alaska, pp. 21–52. https://doi.org/10.1130/SPE198-p21.

Byrne, T., 1982. Structural evolution of coherent terranes in the Ghost Rocks Formation, Kodiak Island. Alaska. Geological Society, London 10, 229–242. https://doi.org/10.1144/GSL.SP.1982.010.01.15. Special Publications.

Clift, P.D., Pavlis, T., DeBari, S.M., Draut, A.E., Rioux, M., Kelemen, P.B., 2005. Subduction erosion of the Jurassic Talkeetna-Bonanza arc and the Mesozoic accretionary tectonics of western North America. Geol 33 (881). https://doi.org/10.1130/G21822.1.

Cloos, M., Shreve, R.L., 1988. Subduction-channel model of prism accretion, melange formation, sediment subduction, and subduction erosion at convergent plate margins: 1. Background and description. PAGEOPH 128, 455–500. https://doi.org/10.1007/BF00874548.

Connelly, W., 1978. Uyak Complex, Kodiak Islands, Alaska: A Cretaceous subduction complex. Geol. Soc. Am. Bull. 89, 755–769.

Ernst, R.E., 2014. Oceanic LIPs: oceanic plateaus and ocean-basin flood basalts and their remnants through time. Large Igneous Provinces. Cambridge University Press, Cambridge, pp. 90–110. https://doi.org/10.1017/CBO9781139025300.004.

Fagereng, A., Sibson, R.H., 2010. Mélange rheology and seismic style. Geology. 38, 751–754. https://doi.org/10.1130/G30868.1.

Farris, D.W., Paterson, S.R., 2009. Subduction of a segmented ridge along a curved continental margin: Variations between the western and eastern Sanak–Baranof belt, southern Alaska. Tectonophysics. 464, 100–117. https://doi.org/10.1016/j.tecto.2007.10.008.

Festa, A., Pini, G.A., Ogata, K., Dilek, Y., 2019. Diagnostic features and field-criteria in recognition of tectonic, sedimentary and diapiric mélanges in orogenic belts and exhumed subduction-accretion complexes. Gondwana Research 74, 7–30. https://doi.org/10.1016/j.gr.2019.01.003.

Fisher, D.M., Byrne, T., 1992. Strain variations in an ancient accretionary complex: Implications for forearc evolution. Tectonics. 11, 330–347. https://doi.org/10.1029/91TC01490.

Fisher, D.M., Tonai, S., Hashimoto, Y., Tomioka, N., Oakley, D., 2019. K-Ar Dating of Fossil Seismogenic Thrusts in the Shimanto Accretionary Complex, Southwest Japan. Tectonics. 38, 3866–3880. https://doi.org/10.1029/2019TC005571.

Frey, F.A., Jones, W.B., Davies, H., Weiss, D., 1991. Geochemical and petrologic data for basalts from sites 756, 757, and 758: Implications for the origin and evolution of Ninetyeast Ridge. Proc. Ocean Drilling Program, Scientific Results 61 32, 611–659. https://doi.org/10.2973/odp.proc.sr.121.163.1991.

Hara, H., Kimura, K., 2008. Metamorphic and cooling history of the Shimanto accretionary complex, Kyushu, Southwest Japan: Implications for the timing of out-of-sequence thrusting. Island Arc 17, 546–559. https://doi.org/10.1111/j.1440-1738.2008.00636.x.

Hilchie, L.J., Jamieson, R.A., 2014. Graphite Thermometry in a Low-Pressure Contact Aureole, 208–209. Lithos, Halifax, Nova Scotia, pp. 21–33. https://doi.org/10.1016/j.lithos.2014.08.015.

Hirano, N., 2011. Petit-spot volcanism: A new type of volcanic zone discovered near a trench. Geochem. J. 45, 157–167. https://doi.org/10.2343/geochemj.1.0111.

Hirano, N., Machida, S., 2022. The mantle structure below petit-spot volcanoes. Commun. Earth. Environ. 3, 1–11. https://doi.org/10.1038/s43247-022-00438-1.

Hirano, N., Machida, S., Sumino, H., Shimizu, K., Tamura, A., Morishita, T., Iwano, H., Sakata, S., Ishii, T., Arai, S., Yoneda, S., Danhara, T., Hirata, T., 2019. Petit-spot volcanoes on the oldest portion of the Pacific plate. Deep Sea Research Part I: Oceanographic Research Papers 154, 103142. https://doi.org/10.1016/j.dsr.2019.103142.

Ikesawa, E., Kimura, G., Sato, K., Ikehara-Ohmori, K., Kitamura, Y., Yamaguchi, A., Ujiie, K., Hashimoto, Y., 2005. Tectonic incorporation of the upper part of oceanic crust to overriding plate of a convergent margin: An example from the Cretaceous–early Tertiary Mugi Mélange, the Shimanto Belt. Japan. Tectonophysics 401, 217–230. https://doi.org/10.1016/j.tecto.2005.01.005.

Jellinek, A.M., Manga, M., 2004. Links Between Long-Lived Hot Spots, Mantle Plumes, D″, and Plate Tectonics. Reviews of Geophysics 42. https://doi.org/10.1029/2003RG000144.

Kiminami, K., Kashiwagi, N., Miyashita, S., 1992. Ocurrence and significance of in-situ greenstones from the Mugi Formation in the Upper Cretaceous Shimanto Supergroup, eastern Shikoku. Japan. Jour. Geol. Soc. Japan 98, 867–883.

Kiminami, K., Miyashita, S., 1992. Occurrence and geochemistry of greenstones from the Makimine Formation in the Upper Cretaceous Shimanto Supergroup in Kyushu. Japan. Jour. Geol. Soc. Japan 98, 391–400.
Kimura, G., Mukai, A., 1991. Underplated unit in an accretionary complex: melange of the Shimanto Belt of eastern Shikoku, southwest Japan. Tectonics. 10, 31–50. https://doi.org/10.1029/90TC00799.
Kimura, G., Yamaguchi, A., Hojo, M., Kitamura, Y., Kameda, J., Ujiie, K., Hamada, Y., Hamahashi, M., Hina, S., 2012. Tectonic mélange as fault rock of subduction plate boundary. Tectonophysics. 568–569, 25–38. https://doi.org/10.1016/j.tecto.2011.08.025.
Kirilova, M., Toy, V., Rooney, J.S., Giorgetti, C., Gordon, K.C., Collettini, C., Takeshita, T., 2018. Structural disorder of graphite and implications for graphite thermometry. Solid Earth 9, 223–231. https://doi.org/10.5194/se-9-223-2018.
Kitamura, Y., Katsushi, S., Ikesawa, E., Ikehara-Ohmori, K., Kimura, G., Kondo, H., Ujiie, K., Onishi, C.T., Kawabata, K., Hashimoto, Y., Mukoyoshi, H., Masago, H., 2005. Mélange and its seismogenic roof décollement: A plate boundary fault rock in the subduction zone—An example from the Shimanto Belt. Japan. Tectonics 24, TC5012. https://doi.org/10.1029/2004TC001635.
Kusky, T.M., Bradley, D.C., 1999. Kinematic analysis of mélange fabrics: examples and applications from the McHugh Complex, Kenai Peninsula. Alaska. Journal of Structural Geology.
Lahfid, A., Beyssac, O., Deville, E., Negro, F., Chopin, C., Goffé, B., 2010. Evolution of the Raman spectrum of carbonaceous material in low-grade metasediments of the Glarus Alps (Switzerland): RSCM in low-grade metasediments. Terra Nova 22, 354–360. https://doi.org/10.1111/j.1365-3121.2010.00956.x.
Mackenzie, J.S., 1989. Geochemical study of the greenstones of the Cretaceous and Paleogene Shimanto accretionary complex in eastern Kyushu: Implications for origin and mode of emplacement. J. Min. Petr. Econ. Geol. 84, 278–292. https://doi.org/10.2465/ganko.84.278.
Maruyama, S., Send, T., 1986. Orogeny and relative plate motions: Example of the Japanese Islands. Tectonophysics, Tectonics of the Eurasian Fold Belts 127, 305–329. https://doi.org/10.1016/0040-1951(86)90067-3.
Matsumura, M., Hashimoto, Y., Kimura, G., Ohmori-Ikehara, K., Enjohji, M., Ikesawa, E., 2003. Depth of oceanic-crust underplating in a subduction zone: Inferences from fluid-inclusion analyses of crack-seal veins. Geol 31, 1005. https://doi.org/10.1130/G19885.1.
Menant, A., Angiboust, S., Gerya, T., Lacassin, R., Simoes, M., Grandin, R., 2020. Transient stripping of subducting slabs controls periodic forearc uplift. Nat. Commun. 11, 1823. https://doi.org/10.1038/s41467-020-15580-7.
Meneghini, F., Moore, J.C., 2007. Deformation and hydrofracture in a subduction thrust at seismogenic depths: The Rodeo Cove thrust zone, Marin Headlands, California. GSA Bulletin 119, 174–183. https://doi.org/10.1130/B25807.1.
Moore, J.C., Byrne, T., 1987. Thickening of fault zones: A mechanism of mélange formation in accreting sediments. Geology. 15, 1040–1043. https://doi.org/10.1130/0091-7613(1987)15<1040: TOFZAM>2.0.CO;2.
Moore, J.C., Byrne, T., Plumley, P.W., Reid, M., Gibbons, H., Coe, R.S., 1983. Paleogene evolution of the Kodiak 266 Islands, Alaska: Consequences of ridge-trench interaction in a more southerly latitude. Tectonics. 2, 265–293.
Moris-Muttoni, B., Raimbourg, H., Augier, R., Champallier, R., Le Trong, E., 2022. The impact of melt versus mechanical wear on the formation of pseudotachylyte veins in accretionary complexes. Sci. Rep. 12, 1–12. https://doi.org/10.1038/s41598-022-05379-5.
Moris-Muttoni, B., Raimbourg, H., Champallier, R., Augier, R., Lahfid, A., Le Trong, E., Di Carlo, I., 2023. The effect of strain on the crystallinity of carbonaceous matter: Application of Raman spectroscopy to deformation experiments. Tectonophysics. 869, 230126. https://doi.org/10.1016/j.tecto.2023.230126.
Müller, R.D., Sdrolias, M., Gaina, C., Steinberger, B., Heine, C., 2008. Long-Term Sea-Level Fluctuations Driven by Ocean Basin Dynamics. Science (1979) 319, 1357–1362. https://doi.org/10.1126/science.1151540.
Munoz-Montecinos, J., Cambeses, A., Angiboust, S., 2024. Accretion and subduction mass transfer processes: Zircon SHRIMP and geochemical insights from the Carboniferous Western Series. Central Chile. International Geology Review 66, 54–80. https://doi.org/10.1080/00206814.2023.2185822.
Osozawa, S., Pavlis, T., Flower, M.F.J., 2011. Sedimentary block-in-matrix fabric affected by tectonic shear, Miocene Nabae complex. In: Wakabayashi, J., Dilek, Y. (Eds.), Mélanges: Processes of Formation and Societal Significance. Geological Society of America, Japan, p. 0. https://doi.org/10.1130/2011.2480(08.
Palazzin, G., Raimbourg, H., Famin, V., Jolivet, L., Kusaba, Y., Yamaguchi, A., 2016. Deformation processes at the down-dip limit of the seismogenic zone: The example of Shimanto accretionary complex. Tectonophysics. 687, 28–43. https://doi.org/10.1016/j.tecto.2016.08.013.
Pavlis, T.L., Monteverde, D.H., Bowman, J.R., Rubenstone, J.L., Reason, M.D., 1988. Early Cretaceous near-trench plutonism in southern Alaska: Atonalite-Trondhjemite Intrusive Complex injected during ductile thrusting along the Border Ranges Fault System. Tectonics. 7, 1179–1199. https://doi.org/10.1029/TC007i006p01179.
Plafker, G., Moore, J.C., Winkler, G.R., Berg, H., 1994. Geology of the southern Alaska margin. The geology of 249 Alaska: Boulder, Colorado, Geological Society of America. Geology of North America 1, 389–449.
Raimbourg, H., Augier, R., Famin, V., Gadenne, L., Palazzin, G., Yamaguchi, A., Kimura, G., 2014. Long-term evolution of an accretionary prism: The case study of the Shimanto Belt, Kyushu, Japan: Long-term evolution of the Shimanto Belt. Tectonics. 33, 936–959. https://doi.org/10.1002/2013TC003412.
Raimbourg, H., Famin, V., Palazzin, G., Yamaguchi, A., Augier, R., 2017. Tertiary evolution of the Shimanto belt (Japan): A large-scale collision in Early Miocene: Early Miocene Collision in Shimanto Belt. Tectonics. 36, 1317–1337. https://doi.org/10.1002/2017TC004529.
Raimbourg, H., Famin, V., Palazzin, G., Yamaguchi, A., Augier, R., Kitamura, Y., Sakaguchi, A., 2019. Distributed deformation along the subduction plate interface: The role of tectonic mélanges. Lithos. 334, 69–87. https://doi.org/10.1016/j.lithos.2019.01.033.
Raimbourg, H., Rajič, K., Moris-Muttoni, B., Famin, V., Palazzin, G., Fisher, D.M., Morell, K., Erdmann, S., Di Carlo, I., Montmartin, C., 2021. Quartz vein geochemistry records deformation processes in convergent zones. Geochemistry, Geophysics, Geosystems 22. https://doi.org/10.1029/2020GC009201.
Rajič, K., Raimbourg, H., Famin, V., Moris-Muttoni, B., Fisher, D.M., Morell, K.D., Canizarés, A., 2023a. Exhuming an Accretionary Prism: A Case Study of the Kodiak Accretionary Complex, Alaska, USA. Tectonics. 42, e2023TC007754. https://doi.org/10.1029/2023TC007754.
Rajič, K., Raimbourg, H., Lerouge, C., Famin, V., Dubacq, B., Canizarès, A., Di Carlo, I., Maubec, N., 2023b. Metamorphic reactions and their implication for the fluid budget in metapelites at seismogenic depths in subduction zones. Tectonophysics. 857.
Rowe, C.D., Moore, J.C., Meneghini, F., McKeirnan, A.W., 2005. Large-scale pseudotachylytes and fluidized cataclasites from an ancient subduction thrust fault. Geol 33, 937. https://doi.org/10.1130/G21856.1.
Rowe, C.D., Moore, J.C., Remitti, F., 2013. The thickness of subduction plate boundary faults from the seafloor into the seismogenic zone. Geology. 41, 991–994. https://doi.org/10.1130/G34556.1.
Sager, W.W., Sano, T., Geldmacher, J., Iturrino, G., Evans, H., Almeev, R., Ando, A., Carvallo, C., Delacour, A., Greene, A.R., Harris, A.C., Herrmann, S., Heydolph, K., Hirano, N., Ishikawa, A., Kang, M., Koppers, A.A.P., Li, S., Littler, K., Mahoney, J., Matsubara, N., Miyoshi, M., Murphy, D.T., Natland, J.H., Ooga, M., Prytulak, J., Shimizu, K., Tominaga, M., Widdowson, M., Woodard, S.C., 2010. In: Proceedings of the IODP, 324. https://doi.org/10.2204/iodp.proc.324.2010. Proceedings of the IODP 324.
Saito, M., 2008. Rapid evolution of the Eocene accretionary complex (Hyuga Group) of the Shimanto terrane in southeastern Kyushu, southwestern. Japan. Island Arc 17, 242–260. https://doi.org/10.1111/j.1440-1738.2008.00615.x.
Saito, T., Okada, Y., Fujisaki, W., Sawaki, Y., Sakata, S., Dohm, J., Maruyama, S., Hirata, T., 2014. Accreted Kula plate fragment at 94Ma in the Yokonami-melange, Shimanto-belt, Shikoku, Japan. Tectonophysics. 623, 136–146. https://doi.org/10.1016/j.tecto.2014.03.026.
Sakai, T., et al., 1984. Microfossil stratigraphy of the Paleogene System in Kyushu Shimanto Belt. Biostratigraphy and International Correlation of the Paleogene System in Japan 95–112.
Sample, J.C., Fisher, D.M., 1986. Duplex accretion and underplating in an ancient accretionary prism, Kodiak Islands. Alaska. Geology 14, 160–163.
Shibata, T., Orihashi, Y., Kimura, G., Hashimoto, Y., 2008. Underplating of mélange evidenced by the depositional ages: U–Pb dating of zircons from the Shimanto accretionary complex, southwest Japan. Island Arc 17, 376–393. https://doi.org/10.1111/j.1440-1738.2008.00626.x.
Taira, A., Katto, J., Tashiro, M., Okamura, M., Kodama, K., 1988. The Shimanto Belt in Shikoku, Japan-Evolution of Cretaceous to Miocene accretionary prism. Modern Geology 12, 5–46.
Taira, A., Okada, H., Whitaker, J.H., Smith, A.J., 1982. The Shimanto Belt of Japan: Cretaceous-lower Miocene active-margin sedimentation. Geological Society, London. Special Publications 10, 5–26. https://doi.org/10.1144/GSL.SP.1982.010.01.01.
Tarduno, J.A., Duncan, R.A., Scholl, D.W., Bonaccorsi, R., Buysch, A., Carvallo, C., Cottrell, R.D., Einaudi, F., Frey, F.A., Gudding, J.A., Haggas, S., Huang, S., Keller, R. A., Kerr, B.C., Lindblom, S., Neal, C.R., Regelous, M., Révillon, S., Siesser, W.G., Steinberger, B., Stoll, J., Thompson, P.M.E., Thordarson, T., Torii, M., Tremolada, F., 2002. In: Proc. ODP, Init. Repts. 197. Ocean Drilling Program, TEXAS A&M UNIVERSITY.
Teraoka, Y., Okumura, K., 1992. Tectonic division and Cretaceous sandstone compositions of the Northern Belt of the Shimanto Terrane, southwest. Japan. Mem. Geol. Soc. Jpn. 38, 261–270.
Toriumi, M., Teruya, J., 1988. Tectono-metamorphism of the Shimanto Belt. Modern Geology 12, 303–324.
Tulley, C.J., Fagereng, A., Ujiie, K., 2020. Hydrous oceanic crust hosts megathrust creep at low shear stresses. Sci. Adv. 6, eaba1529. https://doi.org/10.1126/sciadv.aba1529.
Ujiie, K., Saishu, H., Fagereng, Å., Nishiyama, N., Otsubo, M., Masuyama, H., Kagi, H., 2018. An Explanation of Episodic Tremor and Slow Slip Constrained by Crack-Seal Veins and Viscous Shear in Subduction Mélange. Geophys. Res. Lett. 45, 5371–5379. https://doi.org/10.1029/2018GL078374.
van de Lagemaat, S.H.A., van Hinsbergen, D.J.J., 2023. Plate tectonic cross-roads: Reconstructing the Panthalassa-Neotethys Junction Region from Philippine Sea Plate and Australasian oceans and orogens. Gondwana Research. https://doi.org/10.1016/j.gr.2023.09.013.
Vrolijk, P., Myers, G., Moore, J.C., 1988. Warm fluid migration along tectonic melanges in the Kodiak Accretionary Complex. Alaska. J. Geophys. Res. 93, 10313–10324. https://doi.org/10.1029/JB093iB09p10313.
Wakabayashi, J., 2017. Structural context and variation of ocean plate stratigraphy, Franciscan Complex, California: insight into mélange origins and subduction-accretion processes. Prog. Earth. Planet. Sci. 4, 18. https://doi.org/10.1186/s40645-017-0132-y.
Wakabayashi, J., 2011. Mélanges of the Franciscan Complex, California: Diverse structural settings, evidence for sedimentary mixing, and their connection to subduction processes. In: Wakabayashi, J., Dilek, Y. (Eds.), Mélanges: Processes of Formation and Societal Significance. Geological Society of America, p. 0. https://doi.org/10.1130/2011.2480(05.
Yamaguchi, A., Ujiie, K., Nakai, S., Kimura, G., 2012. Sources and physicochemical characteristics of fluids along a subduction-zone megathrust: A geochemical

approach using syn-tectonic mineral veins in the Mugi mélange. Shimanto accretionary complex. Geochemistry, Geophysics, Geosystems 13. https://doi.org/10.1029/2012GC004137.